Numerical Simulation for Combined Blast & Fragment Effects on RC Slabs

†Shengrui Lan and Kenneth B. Morrill

Karagozian & Case, Inc., 700 N. Brand Blvd., Suite 700, Glendale, CA 91203, USA

†Corresponding author: lan@kcse.com

Abstract

The objective of this study is to evaluate the residual loading capacity of the damaged RC slabs by the combined blast and fragment loading (CBFL) effects. High-fidelity physics-based (HFPB) finite element analysis technique is used for the numerical simulations in this study, which takes into account material nonlinearity, strain rate effects, large deformation behavior, "real time" blast and fragment loading, and actual supporting boundary conditions. Numerical model and simulation techniques have been validated through five tests including the quasi-static tests, the blast loading only test and the CBFL tests, in comparison of the deformation and pristine/residual loading capacity of the RC slabs, which was carried out without knowing the test results. Using a fast running tool, fragments and blast loading are generated on full scale RC slabs. A parametric study has been done to investigate dynamic response of the full-scale RC slabs under CBFL effects.

Keywords: Blast loading, fragment loading, RC slab, dynamic response, residual capacity.

Introduction

When a cased munition or an improvised explosive device (IED) detonates nearby a structure, the structure is subjected to a combination of blast and fragment loading (CBFL). Dynamic response of reinforce concrete (RC) slabs under the CBFL may be different from that under the air blast loading. Some studies have been done in this area for the formation of fragments loading and their effects on the structural members, e.g., the works reported in reference [1-5]. A series of small scale experiments using bare charge with pre-formed ball bearings were conducted by Swedish Research Institute (FOI) to investigate the effects of the combined blast and fragment loadings [4]. The objective of the study was to develop a fast running tool to account for the fragmentation effect on the doubly reinforced concrete slab. As part of the study, numerical simulations were conducted for five of the experiments. This paper will focus on the numerical simulation to predict the residual capacity of the RC slabs after CBFL effect.

High-fidelity physics-based (HFPB) finite element analysis (FEA) technique is used for the simulations in this study, which can take into account many physical behaviors of materials and structures, such as: (a) material nonlinearity and geometry nonlinearity (large deformation); (b) dynamic strain rate effects for material strength increase; (c) structural 3D behavior with complex stress states – not only flexural but also axial, shear and torsional behaviors/responses; (c) multi-components with multi-materials and structural details for connections – not only global but also localized response; (d) "Real time" blast loading – blast loads are generally applied with different arrival times and pressure time histories at different locations (i.e., non-uniform loading); (e) more realistic boundary conditions of the structure, instead of the artificial boundary conditions in SDOF model.

LS-DYNA (www.lstc.com) is used for the simulations in this study. LS-DYNA is a general-purpose finite element program capable of simulating complex dynamic structural problems, which has been widely used in blast and impact effects analysis communities.

K&C concrete material model (i.e., MAT_072 in LS-DYNA) has been incorporated in LS-DYNA, which enables that more reliable analysis results can be obtained for reinforced concrete (RC) structures under blast and impact effects. This is because this concrete model has implemented many key features of concrete materials: (a) three-invariant strength surfaces to reflect the pressure-dependent and difference in triaxial extension and compression; (b) effects of confinement - compressive strength is significantly enhanced by confinement; (c) non-linearity - Elastic, plastic with hardening and softening (or damage), for which a damage metric is used in K&C model to gauge the evolution; (d) strain rate effects – significant material strength enhancement by high strain rate, which is important for blast loading effects where the concrete strength could be more than doubled; (e) Fracture energy – important tensile behavior of concrete; (f) Shear-dilatancy – Concrete's expansion upon cracking provides increased strength /ductility where confinement is adequate.

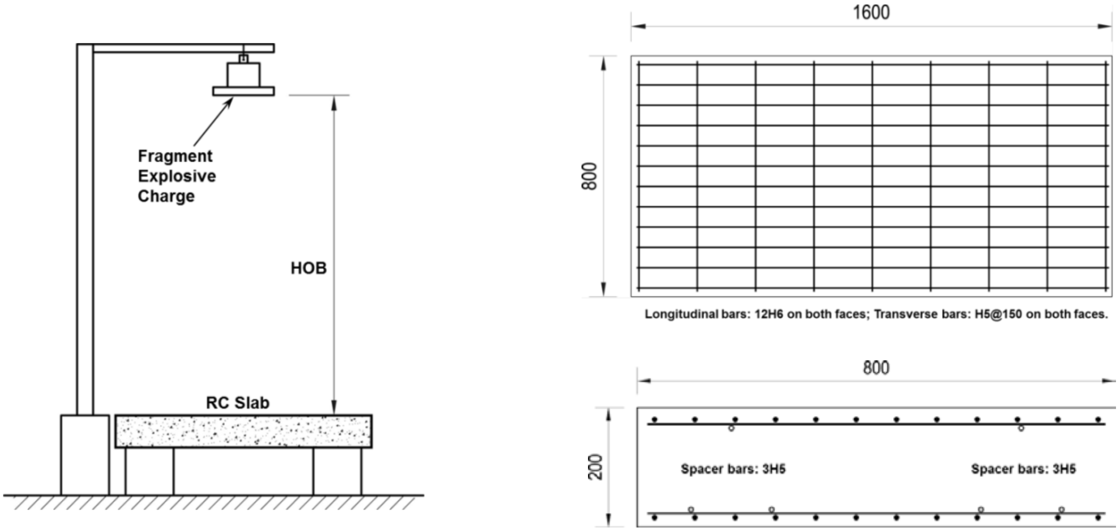

Figure 1. Test set-up and RC slab specimen.

RC Slab Tests Under Fragment Loading

A series of test has been conducted for RC slabs using the test set-up shown in Figure 1 [4]. Tables 1 and 2 summarize the information about the specimens and test data from five tests, which include two quasi-static loading (QSL) tests of the pristine slabs, two fragment loading tests followed by QSL tests of the damaged slabs for the residual capacity, and one test under CBFL.

Three approaches were taken using three types of set-ups: (a) the QSL test (three point loading flexural test) for loading capacity of the pristine slab specimens as a baseline control, (b) expose the specimens to the fragments loading then conduct QSL test of the damaged slabs for their residual loading capacity, and (c) Expose the specimens to the CBFL effects and record dynamic displacement histories; QSL test was not conducted for the damaged slab.

Table 1. Test specimens of RC slabs for quasi-static and dynamic tests.

Test No.	Slab No.	Spacer bar	Concrete Strength (MPa)		Pristine Capacity (kN)	Residual Capacity (kN)	Loading
			Cube	Cylinder			
24	20	No	39.9	31.9	178	-	Quasi-static
40	19	One side	43.2	34.5	183	-	Quasi-static.
19	18	Both sides	37.3	29.8	-	172	Fragment
41	16	Both sides	37.9	30.3	-	185	Fragment
52	22	No	33.2	26.6	-	-	Blast & Fragment

Note: a) The dimension of all slabs is 1600 x 800 x 200 mm. b) Longitudinal bars in all slabs are 12Φ6 as shown in Figure 1.

Table 2. Dynamic test results under fragment explosive charges.

Test No.	Charge Weight (kg)	Fragment size (mm)	No. of Balls	Height of Burst (m)	Average Velocity from Test (m/s)	Fragment Density (kg/m^2)
19	8.847	Φ8	345	2.1	1,880	0.25
41	8.969	Φ8	346	1.9	1,880	0.30
52	8.877	Φ8	345	2.7	1,815	0.17

Blind Prediction of Test Results

Quasi-static Loading for Pristine Slabs

Two QSL tests (i.e., Test 24 and Test 40 in Table 1) were conducted for the pristine slabs as the baseline control data. The loading capacity was evaluated through three points loading flexural test on the simply supported slabs as shown in Figure 2. In those tests, the slabs were loaded quasi-statically till all the bottom longitudinal rebars fractured, which captured the post-peak low strength as well.

(a) Test 24 as described in Table 1.

(b) Test 40 as described in Table 1.

Figure 2. Two quasi-static tests for the pristine slabs.

Finite element models have been developed for the five specimen slabs (Table 1) to simulate the tests. As an example, simulation results for test 24 presented in Figure 3 show that concrete damage is concentrated at the middle span of the slab and rebars are fractured, which agrees the test failure mode shown in Figure 2a. The predicted loading capacities of 165 kN (Figure 4a) in Test 24 and 185 kN in Test 40 are quite close to the test results of 178 kN in Test 24 and 183 kN in Test 40, respectively. Those simulation results indicate the numerical model developed for the slab QSL test is valid. In addition, the predicted loading capacities of the five pristine slabs (Table 1) are presented in Figure 4b, which indicate the spacer bars have some influence.

Fragment Loading Effects

Two tests (i.e., Test 19 and Test 41) were carried out by the fragment loading for dynamic response and then QSL on the damaged slabs for their residual capacities. The tested specimen of Test 41 is shown in Figure 5. These two tests are simulated with following procedures: Step 1: Gravity loading is applied from 0 to 100 ms (t1); Step 2: Blast/fragment loading is applied from 100 to 200 ms (t2), where the fragments' velocities and positions are outputted from the fragment explosive charge simulation described in the previous section according to the height of burst in Table 2 and mapped on the test specimens; and Step 3:

Posttest QSL with a displacement loading on the loading bar of 50 mm/s from 200 ms until the rebars fracture.

The simulation results for Test 41 in Figure 6 indicate that fragment damage is mainly on the top surface of the slab and the failure of the damaged slab in QSL simulation is due to rebar fracture. The residual capacity and the pristine capacity of the slab are compared in Figure 6d, which indicates that the residual capacity is about 91% of the pristine capacity. This is probably because the loading capacity is governed by the rebar fracture and the concrete damage has relatively less influence to the loading capacity.

An interesting observation from the simulation on the residual capacity is the damaged slab behaved more ductile than the pristine slabs, i.e., the force-displacement curve has a clear “softening” stage, instead of dropping immediately to the lowest value in the pristine slab as shown in Figure 6d. This is probably because all rebars in the pristine slabs are at the same stress status and break at the same time, whereas the rebars may be in slightly different stress status and break at the different time due to the non-uniform damage of concrete.

From the simulation results for Test 19, the same observations and conclusions can be drawn as those in Test 41. The residual capacity of the damage slab in Test 19 is about 88%. A comparison of the predicted results and test results in Table 3 indicates that the numerical model can reasonably predict the loading capacity of the damaged slabs. In addition, the fragment damage in these two cases doesn’t significantly reduce the loading capacity of the slabs.

Slab Response by Combined Blast and Fragment Loading

Displacement-time histories from the simulation results of Test 52 are presented in Figure 7, which indicates the response of the slab specimen under the CBFL is basically a significant rebound and followed by some oscillations. The rebound displacement was not captured during the CBFL test, which is probably the displacement gages were not set for the rebound displacement. Nevertheless, it may be considered that the predicted overall response is still reasonable when compared to the entire global response curves from test (Figure 7a) and simulation (Figure 7b).

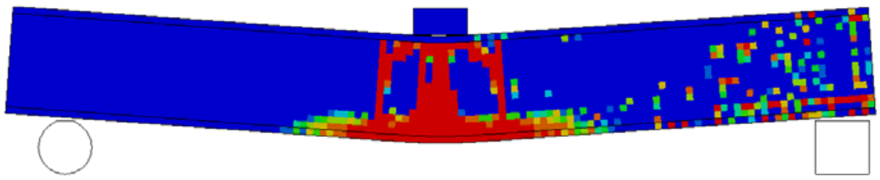

(a) Concrete damage at failure.

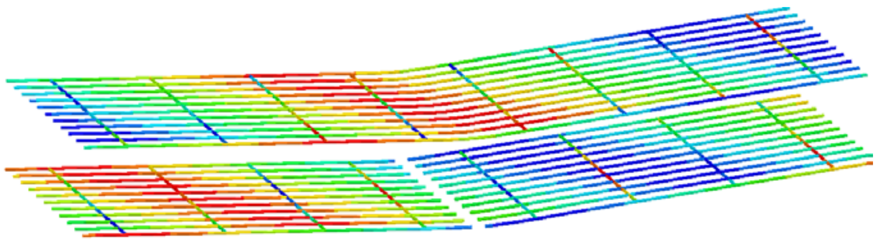

(b) Rebar fracture.

Figure 3. Simulation of quasi-static loading test for pristine slab - Test 24.

Table 3. Comparison of loading capacity from pristine and fragment damaged slabs.

Test	Pristine slab (predicted)	Damaged slab (predicted)	Damaged slab (Test)	Percentage of Residual Capacity
Test 19	205	180	172	88%
Test 41	200	182	185	91%

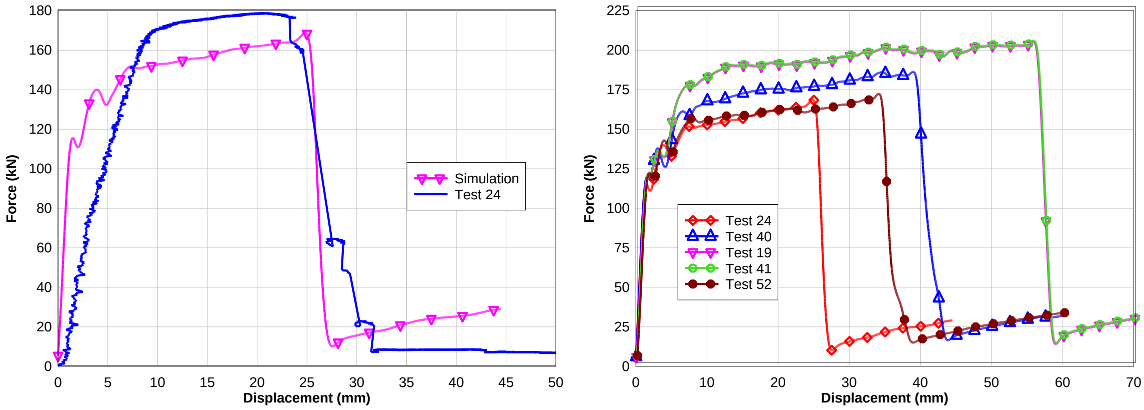

(a) Test 24 (b) All five specimens.

Figure 4. Loading capacity of pristine slabs in five tests.

(a) Damaged by the fragment loading.

(b) Failure in quasi-static test for the damaged slab.

Figure 5. Test 41 – slab under fragment loading and posttest quasi-static test.

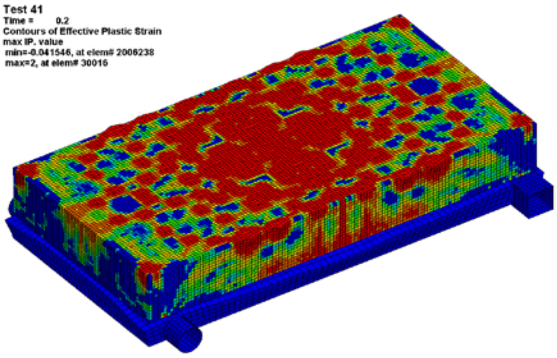

(a) Damage by fragment loading

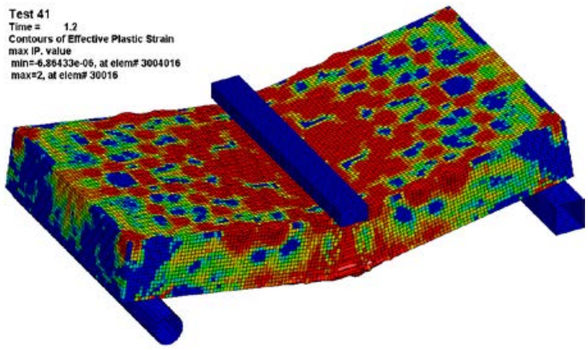

(b) Failure model after QSL

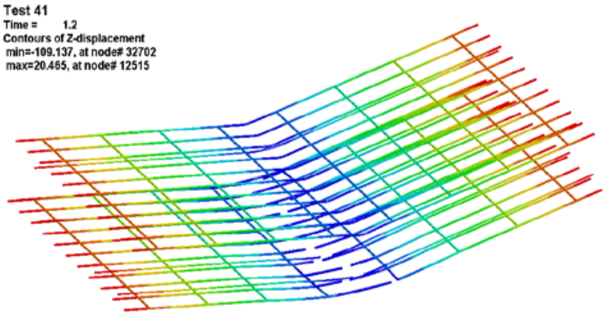

(c) Rebar fracture in QSL

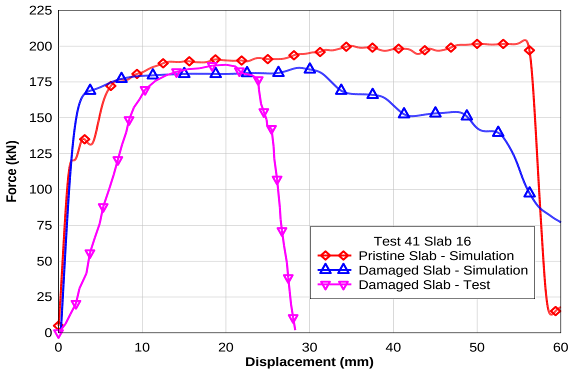

(d) Compare loading capacity

Figure 6. Simulation results for Test 41.

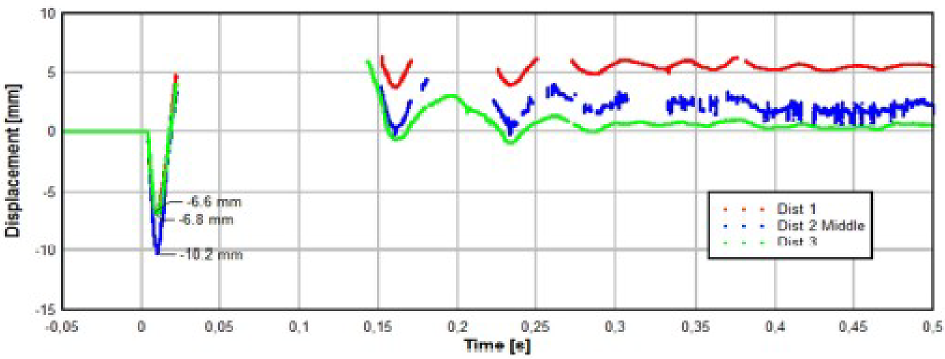

(a) Test measurement.

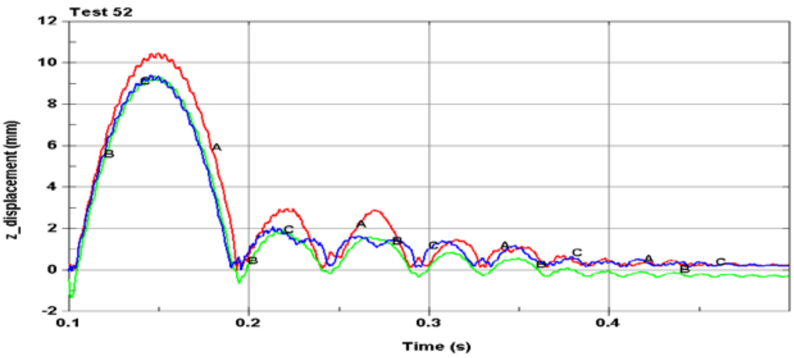

(b) Simulation

Figure 7. Test and simulation results for Test 52.

Parametric Study

Case Description

Following the successful validation of the numerical model described in the foregoing sections, this section summarizes the simulation results from the ten cases for a parametric study. The ten cases are defined in Table 4, including Cases D1 to D5 for Bomb B and Cases E1 to E5 for Bomb C at different standoff distances and different orientation angles α (Figure 8). The slabs to be analyzed are 3.0 m long by 1.6 m wide, while their thickness and reinforcement bars (rebars) are different in the two series as shown in Table 4. Concrete of the slabs is Grade C32/40 (f'_c= 32 MPa), and the rebar is Grade 500C (fy = 500 MPa).

The fragment loading from these two bombs are calculated by KC-Frag [5], which has been developed by K&C for characterizing fragment loading from a pipe bomb. The blast loading for the two cases is calculated based on the reduced charge weight, which is determined by the Fano Equation [9]:

$$\frac{W_1}{W} = 0.2 + \frac{0.8}{1 + \frac{M}{C}}$$

Where, W1/W is the ratio of the reduced charge weight to the actual charge weight;
M/C is the case to charge weight ratio.

The loading characteristics from these ten cases are summarized in Tables 5 and 6. The two key parameters are the total momentums due to air blast and fragments, which is usually dominant the damage of the RC slabs. The total momentum due to fragments is much greater than that due to air blast in all cases, which indicates that the fragment loading may produce greater damage on the slab.

The fragment loading for each fragment generated by KC-Frag is a triangle pressure pulse with a high pressure peak and a short duration based on the momentum from a fragment, which will be applied to a single element. About two thousands of loading curves calculated from the effective charge weight are generated and mapped on the slabs to mimic the "real time" blast and fragment loading as each load curve has its own arrival time, peak pressure and duration.

Table 4. Parameters of the ten cases.

Case No.	Bomb (Effective Charge)	Orientation Angle, *a*	Standoff (m)	Scaled Distance (m/kg$^{1/3}$)	Slab Dimension & Reinforcements
D1	Bomb B (46.05 kg)	0^o	5	1.395	3.0 x 1.6 x 0.6 m (clear span = 2.8m) Longitudinal rebars: 11H16 (150 mm c/c) Transverse rebars: 15H10 (200 mm c/c)
D2		10^o	5	1.395	
D3		17^o	5	1.395	
D4		0^o	7.5	2.092	
D5		0^o	10.0	2.790	
E1	Bomb C (2.29 kg)	0^o	2.8	2.124	3.0 x 1.6 x 0.25 m (clear span = 2.8m) Longitudinal rebars: 16H13 (100 mm c/c) Transverse rebars: 15H10 (200 mm c/c)
E2		10^o	2.8	2.124	
E3		17^o	2.8	2.124	
E4		0^o	5.0	3.793	
E5		0^o	7.5	5.690	

Note: Concrete is grade C32/40 (fpc f_c' = 32 MPa); Reinforcement bar is Grade 500C (f_y=500 MPa).

Table 5. Summary of blast and fragment loading for Cases D1 to D5 with Bomb B.

Description	D1	D2	D3	D4	D5
Standoff (m)	5	5	5	7.5	10
Orientation (degree)	0	10	17	0	0
Charge Explosive Weight (kg)			90		
Casing Weight (kg)			141		
Reduction Factor			0.512		
Reduced Charge Weight (kg)			46.05		
Peak AirBlast Pressure (MPa)	1.82	1.82	1.82	0.51	0.24
Peak AirBlast Impulse (MPa-msec)	1.65	1.65	1.65	1.01	0.73
Total Momentum due to AirBlast (N-sec)	7633	7633	7633	4704	3477
Total number of fragment	1184	764	298	798	602
Smallest fragment weight impacting slab (g)	0.16	0.17	0.17	0.16	016
Largest fragment weight impacting slab (g)	139	102	85	139	139
Total fragment weight impacting slab (g)	7827	5594	2289	5432	4044
Lowest fragment normal impact velocity (m/s)	868	875	850	868	868
Highest fragment normal impact velocity (m/s)	3499	3445	3078	3499	3499
Average fragment normal impact velocity (m/s)	2171	2137	2079	2184	2179
Fragment velocity per Gurney Equation (m/s)			2187		
Average fragment impact momentum (N-sec)	14.2	15.7	15.9	14.5	14.8
Total Momentum due to Fragment (N-sec)	16861	12029	4738	11571	8875

Finite Element Model

The finite element models for Cases D1 to D5 (Model D) and Cases E1 to E5 (Model E) are shown in Figures 9 and 10, respectively. In these models, 25 mm cube solid elements are employed for concrete material and 25 mm long beam elements are employed for reinforcement bars.

Fragment Loading

As an example, the blast and fragment loading in Case D1 and D2 is shown in Figures 10, which provide information about the fragment distribution on the slab and the momentum of each fragment. This figures also clearly exhibit how the orientation angle influences the fragment distribution on the slab, i.e., when the orientation angle increases, the affected area reduced from the entire top face (Figure 10c) to about two third (Figure 10d). The key parameters of the blast and fragment loading in Cases D1 to D5 summarized in Table 5 indicate that the total number of fragments and the total momentum due to the fragments are significantly reduced from Case D1 to Case D3, while the average normal impact velocities of the fragments are almost identical. Table 5 also indicates that the fragments numbers are reduced when the standoff distance is increased in Case D4 and D5 in comparison with Case D1.

The key parameters of the fragment loadings in Cases E1 to E5 are summarized in Table 6 and exhibit the same characteristics as in Case D1 to D5 mentioned in the above paragraph.

As each fragment loading is represented by a triangle pressure pulse, a lot of loading curves are generated according to the total number of fragments in Tables 5 and 6 (i.e., from 73 to 1184) and applied on the slab, where applicable.

Table 6. Summary of blast and fragment loading for Cases E1 to E5 with Bomb C.

Description	E1	E2	E3	E4	E5
Standoff (m)	2.8	2.8	2.8	5.0	7.5
Orientation (degree)	0	10	17	0	0
Charge Explosive Weight (kg)			7		
Casing Weight (kg)			37		
Reduction Factor			0.327		
Reduced Charge Weight (kg)			2.29		
Peak AirBlast Pressure (MPa)	0.49	0.49	0.49	0.12	0.057
Peak AirBlast Impulse (MPa-msec)	0.355	0.355	0.355	0.186	0.117
Total Momentum due to AirBlast (N-sec)	1568	1568	1568	886	555
Total number of fragment	431	320	73	272	194
Smallest fragment weight impacting slab (g)	0.26	0.31	0.31	0.26	0.26
Largest fragment weight impacting slab (g)	224	224	194	194	127
Total fragment weight impacting slab (g)	5471	4290	1053	3707	2589
Lowest fragment normal impact velocity (m/s)	148	145	269	148	148
Highest fragment normal impact velocity (m/s)	2587	2547	2070	2586	2586
Average fragment normal impact velocity (m/s)	1356	1355	1318	1378	1393
Fragment velocity per Gurney Equation (m/s)			1355		
Average fragment impact momentum (N-sec)	17.0	18.2	19.7	18.6	18.2
Total Momentum due to Fragment (N-sec)	7343	5820	1436	5064	3534

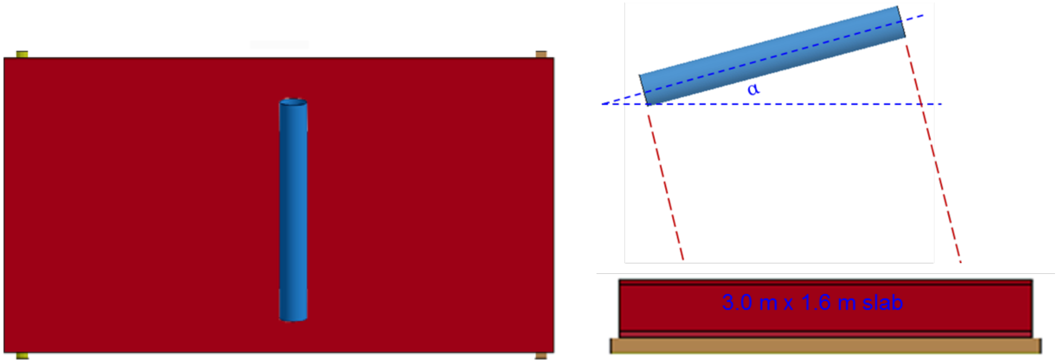

Figure 8. Model for parametric study (not to scale).

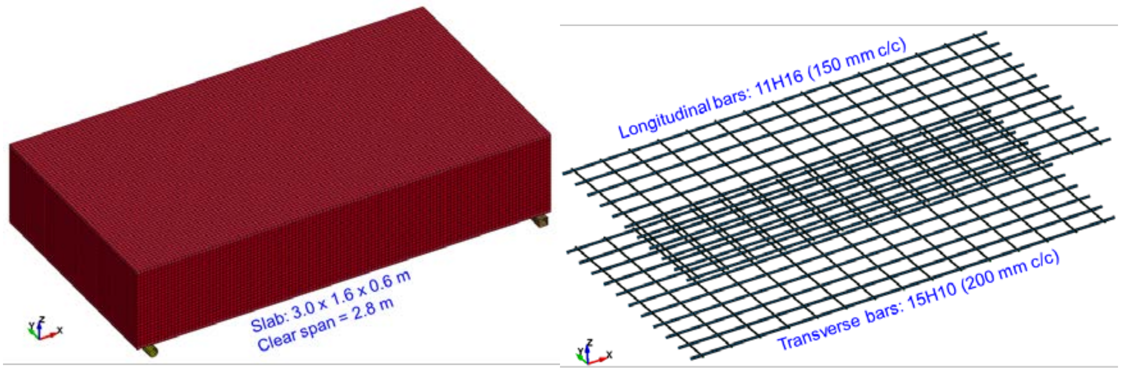

Figure 9. Finite element model for Cases D1 to D5.

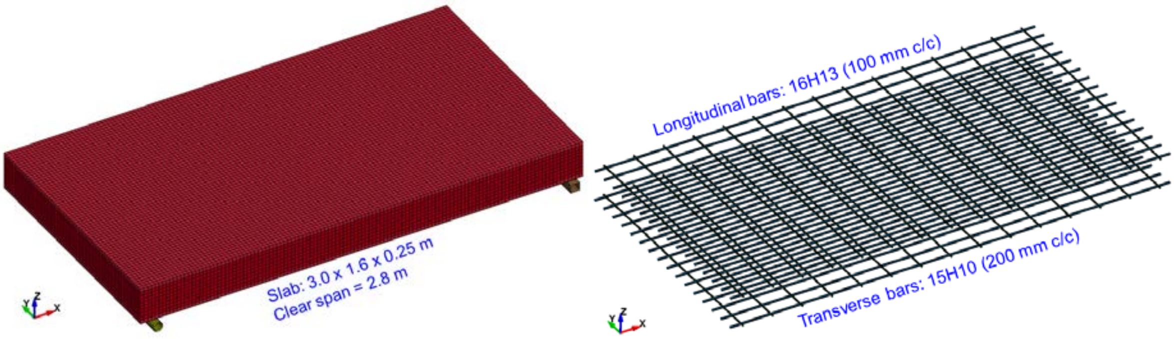

Figure 10. Finite element model for Cases E1 to E5.

Analysis Results

Analysis Results for Cases D1 to D5

The analysis results from Case D1 are presented in Figures 11. The analyses results exhibit that the fragment loading dominates the slab damage, e.g., the entire top face of the slab is damaged by the fragments in Case D1, which results in only 39% of residual capacity of the damaged slab (Table 7). In Case D2, the fragments hit only about two third of the top face and only this area is badly damaged (Figure 12), which results in 42% of residual capacity. In Case D3, nearly one third of the top face is badly damaged by fragments and the damaged slab remains 95% residual capacity. From the QSL simulations for the damaged slabs (Figures 11 and 12), all slabs lose their loading capacities due to the concrete shear failure without rebar fracture in Cases D1 to D3.

When the standoff distance is increased in Cases D4 and D5 compared to Case D1, both blast and fragment momentums decrease significantly (Table 5). Consequently, the concrete damage is less severe and the slab residual capacity in these two cases are increased significantly, i.e., 75% in Case D4 and 83% in Case D5 (Table 7).

The loading capacities of the pristine and damaged slabs shown in Figure 13 indicate that the slab residual capacity in Case D1 and D2 is less than a half of the pristine capacity and the residual capacity in Case D3 has no significant reduction. In Cases D4 and D5, substantial residual capacities still exist. Furthermore, the loading capacity of the damaged slab by blast loading only has almost no reduction compared to the pristine slab.

Table 7 summarizes the loading capacities, the peak dynamic displacements and corresponding support rotation angle [4] in Cases D1 to D5. A relationship between the support rotation and residual capacity is plotted in Figure 13, which indicates that the residual capacity of the damaged slabs can be significantly reduced (less than 50%) when the support rotation is greater than 0.7 degree.

Table 7. Loading capacities of pristine and damaged slabs for Case D1 to D5.

	Loading Capacity (kN)						
	Pristine	Blast	D1	D2	D3	D4	D5
Value	1800	1800	710	763	1710	1346	1497
percentage	100%	100%	39%	42%	95%	75%	83%
D_{max} (mm)	-	1.4	24	19	6	7.6	5.2
θ_{max}		0.05^0	0.98^0	0.78^0	0.25^0	0.31^0	0.21^0

Note: D_{max} = the peak dynamic displacement at the slab center.
θ_{max} = the maximum support rotation angle (degree).

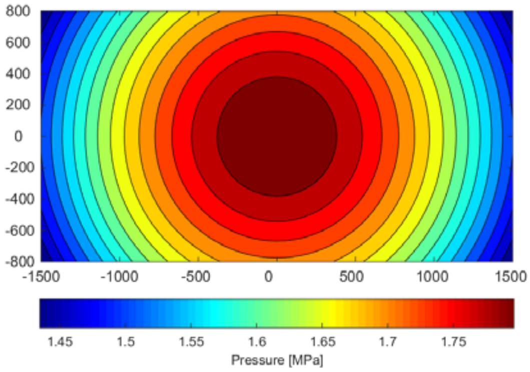

(a) Peak pressure.

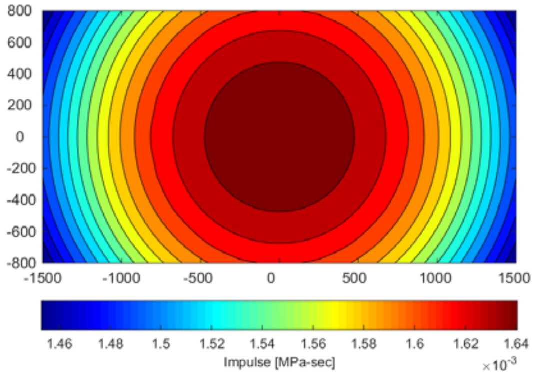

(b) Maximum Impulse.

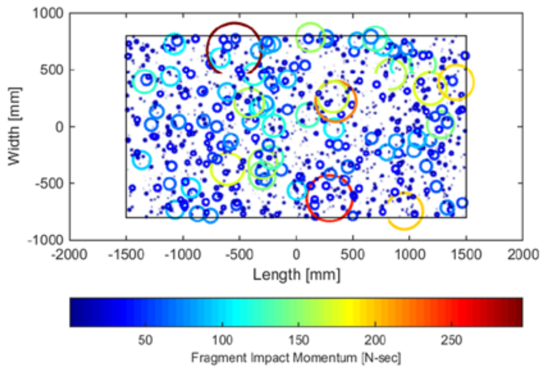

(c) Fragment Loading in Case D1.

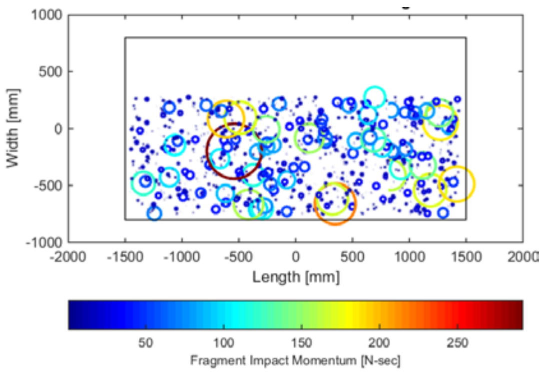

(d) Fragment Loading in Case D2.

Figure 11. Blast and fragment loading distribution in Cases D1 and D2.

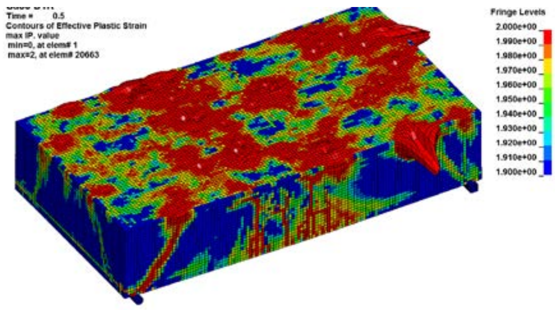

(a) Damage by CBFL

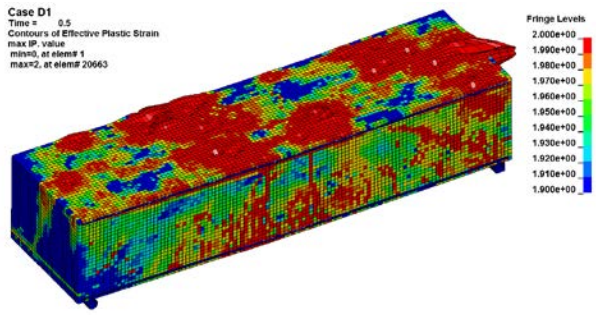

(b) Damage by CBFL (view through the middle section).

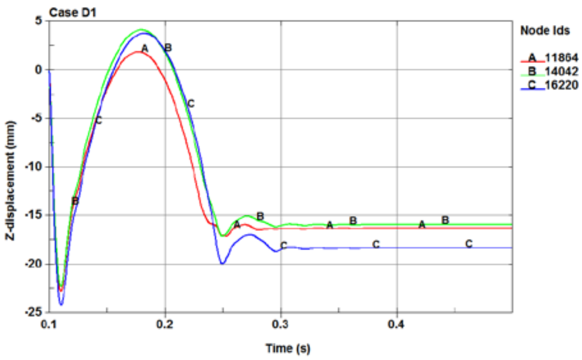

(c) Displacement history (B – middle span; A and C – at quarter spans on left and right, respectively).

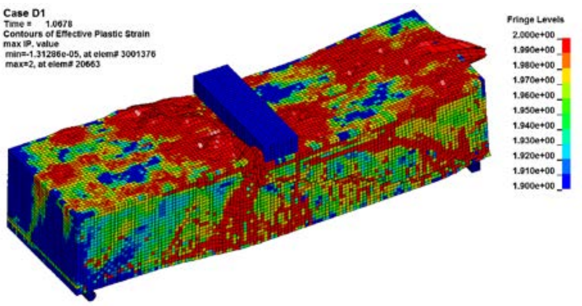

(d) Failure of the damaged slab in posttest QSL (view through the middle section).

Figure 12. Case D1: slab response under CBFL (Continued).

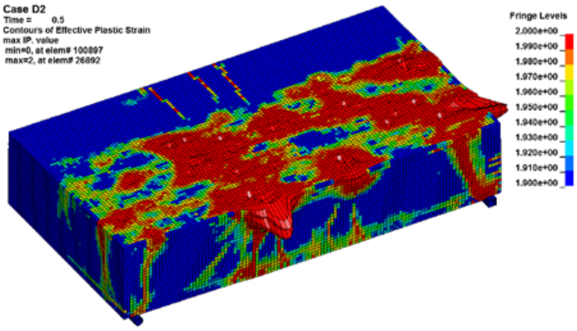

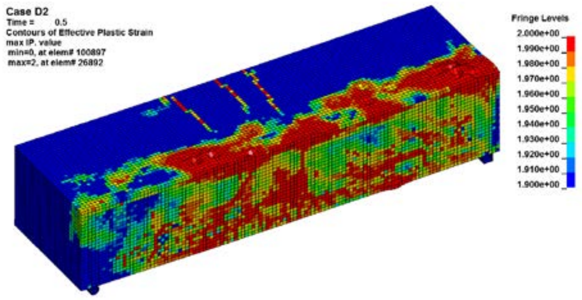

(a) Damage by CBFL (b) Damage by CBFL (view through the middle section).

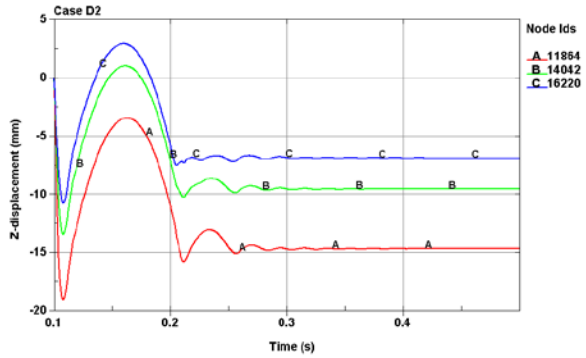

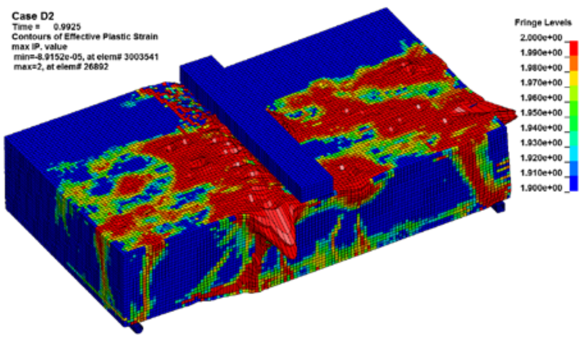

(c) Displacement history (B – middle span; A and C – at quarter spans on left and right, respectively).

(d) Failure of the damaged slab in posttest QSL (view through the middle section).

Figure 13. Case D2: slab response under CBFL.

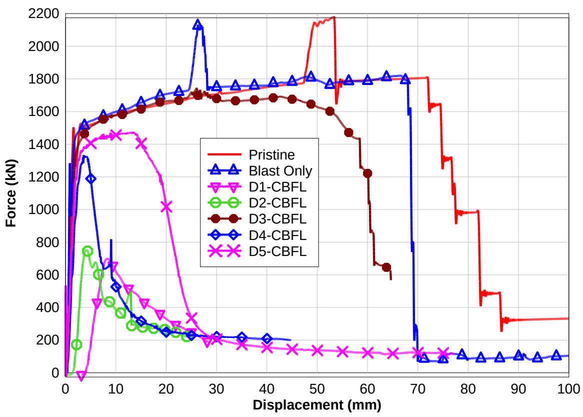

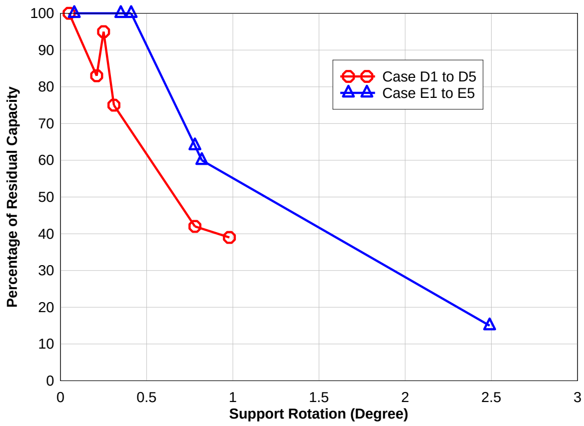

(a) Loading Capacity (b) Support rotation vs. residual capacity.

Figure 14. Loading capacities of pristine and damage slabs in Cases D1 to D5.

Analysis Results for Cases E1 to E5

As an example, the blast and fragment loadings on the slab is shown in Figure 14 and the analysis results from Cases E1 are presented in Figures 15. In Case E1, the slab damage is in the middle along the longitudinal span as the fragment loading distribution from Bomb B (Figure 14b). However, the right side of the slab (Figures 15a) undergoes severer damage due to larger fragment momentum in this area as shown in Figure 4-14b. Damage patterns from other cases are not shown here.

The analysis results summarized in Table 8 indicate that the residual capacities of the damaged slabs in Cases E1, E2 and E4 are 15%, 60% and 64%, respectively, when compared to the pristine slab. The damaged slabs in Cases E3 and E5 and by blast loading only have almost the same loading capacity with the pristine slab. The relationship between the support rotation and the residual capacity in Figure 16 indicates that the slabs lose about 50% loading capacity when the support rotation is greater than 1.2 degree.

When the standoff distances are increased in Case E4 and E5, the global damage to the slab is less significant compared with that in Case E1, although a fragment near the slab edge may cause severe local damage (Figure 16).

The loading capacities of the pristine and damaged slabs are evaluated and their load displacement curves are presented in Figure 17. Similar with Cases D1 to D3, from the failure model of the damaged slab in posttest QSL, all slabs lose the loading capacity due to concrete shear failure and no reinforcement bars fracture.

Table 8. Loading capacities of pristine and damaged slabs for Case E1 to E5.

	Loading Capacity (kN)						
	Pristine	Blast	E1	E2	E3	E4	E5
Value	460	460	70	273	458	295	470
Percentage	100%	100%	15%	60%	100%	64%	100%
D_{max} (mm)	-	2	61	20	8.5	19	10
θ_{max}		0.08^0	2.49^0	0.82^0	0.35^0	0.78^0	0.41^0

Note: D_{max} = the peak dynamic displacement at the slab center.
θ_{max} = the maximum support rotation angle (degree).

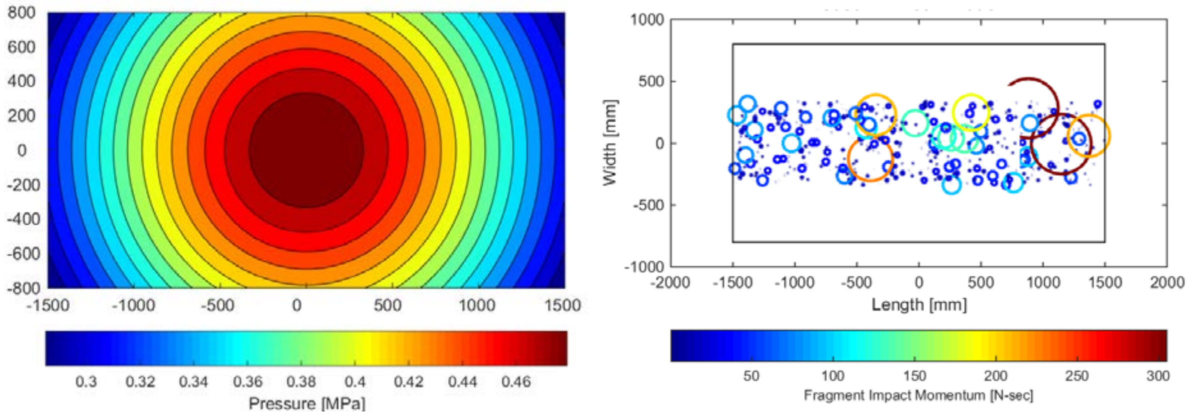

Figure 15. Case E1: Blast and fragment loading on slab.

Conclusions

In this study, the HFPB finite element techniques and procedures for evaluating the residual capacities of RC slabs after the combined blast and fragment loading effects have been validated. A parameter study has been conducted to evaluate the residual capacity of the RC slabs subjected to various blast and fragment loadings. The calculated loading shows the total momentum from fragments can be greater than that from air blast loading generated by pipe bombs. The simulation results show that the fragment loading can dominate the damage of the RC slabs and their residual capacities.

Acknowledgement

The authors acknowledge the financial and technical support by Defence Science & Technology Agency (DSTA) and Nanyang Technological University (NTU).

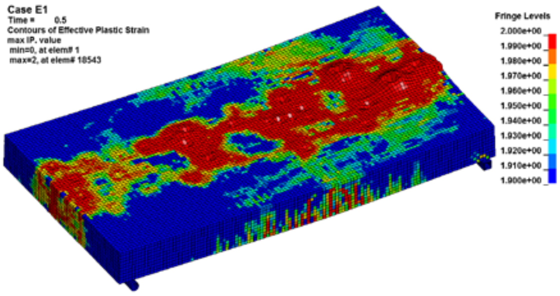

(a) Damage by CBFL

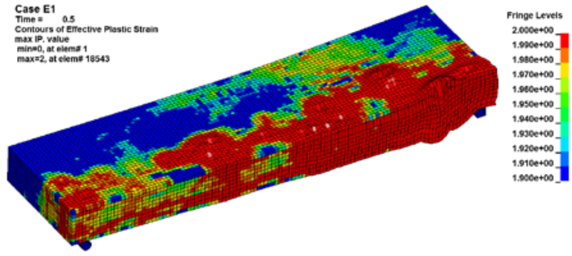

(b) Damage by CBFL (view through the middle section).

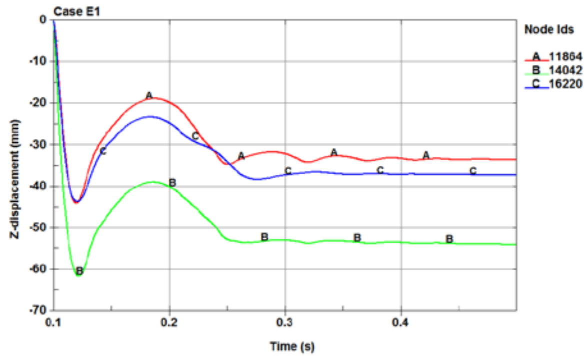

(c) Displacement history (B – middle span; A and C – at quarter spans on left and right, respectively).

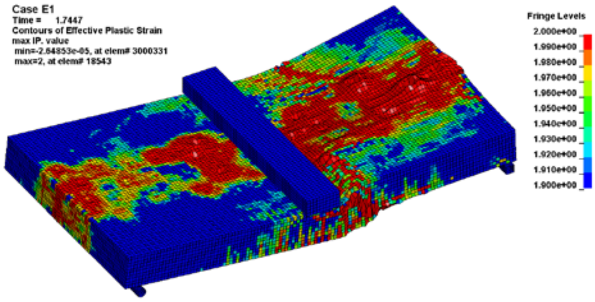

(d) Failure of the damaged slab in posttest QSL (view through the middle section).

Figure 16. Case E1: slab response under CBFL.

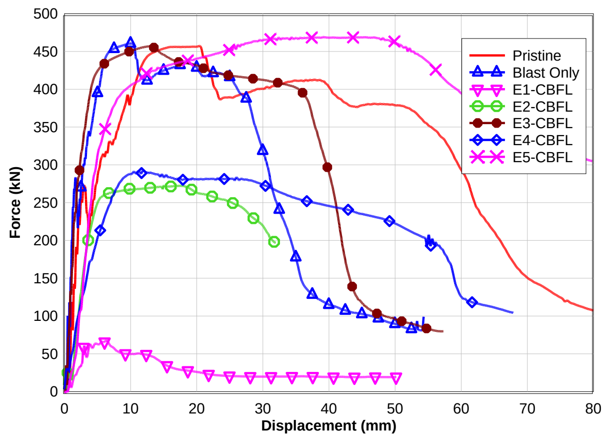

Figure 17. Loading capacities of pristine and damage slabs in Cases E1 to E5.

References

[1] Karpenko, A. and Ceh, M. (2007, April), Experimental simulation of fragmentation effects of an improvised explosive device. 23rd International Symposium on Ballistics, 1413-1420.

[2] Nordstrom, M. and Forsen, R. Damage to reinforced concrete slabs due to fragment loading with different fragment velocities, fragment areal densities and sizes of fragments. National Defense Research, FOA Report S-172-90, Sundyberg, Sweden.

[3] Forsen, R., & Nordstrom, M. (1992, September). Damage to reinforced concrete slabs due to the combination of blast and fragment loading. FOA Report B 20101-2.6, Tumba, Sweden.

[4] Forsén, R., Response to RC Slabs Subjected to Combined Blast and Fragment Loading, Fifth Internal conference on Design and Analysis of Protective Structures, May 2015, Singapore

[5] Crawford, J. E., Fu, S., Magallanes, J. M., and Zhang, Y. "Determining the Effects of Cased Explosives on the Response of RC Columns" for the MABS21, Jerusalem, Israel, October 3-8, 2010.

[6] Joseph M. Magallanes, Youcai Wu, Shengrui Lan, and John E. Crawford, “Parameters Influencing Finite Element Results for Concrete Structures”, ACI SP-306-1, 2016.
[7] Malvar, L. J., Crawford, J. E., Wesevich, J. W., and Simons, D. “A Plasticity Concrete Material Model for DYNA3D”, Int. J. Impact Engng, Vol. 19, Nos. 9-10. pp. 847-873, 1997.
[8] Lan, S., Lim, H. S., Ow, M. C., and Morrill, K. B. "Reinforced Concrete Slab Under Combined Blast and Fragment Loading," for the 16th International symposium on the Interaction of the Effects on Munitions with Structures, Florida, November 9-13, 2015
[9] Fisher E.M., “The Effects of the Steel Case on the Air Blast from High Explosives”, U.S. Nabal Ordnance Laboratory, White Oak, Maryland, February 1953.
[10] U.S. Department of Defense UFC 3-340-02 - "Structures to Resist the Effects of Accidental Explosions", Dec. 2008. (Previously Known as TM5-1300).